JOURNAL OF PROPULSION AND POWER
Vol. 33, No. 2, March–April 2017

Supercritical Mixing and Combustion of Liquid-Oxygen/ Kerosene Bi-Swirl Injectors

Xingjian Wang* and Vigor Yang†
Georgia Institute of Technology, Atlanta, Georgia 30332

DOI: 10.2514/1.B36262

The mixing and combustion characteristics of liquid-oxygen/kerosene bi-swirl injectors are investigated under the supercritical conditions typical of contemporary rocket engines. The basis of the study is a large-eddy simulation technique combined with a unified treatment of real-fluid thermodynamics. The turbulence/chemistry interaction is treated using a laminar flamelet library approach. Emphasis is placed on the near-field flow and flame development downstream of the inner swirler. The flame is found to be stabilized by two counter-rotating vortices in the wake region of the liquid-oxygen post, which is covered by the kerosene-rich mixture. The width of the kerosene annulus is found to significantly affect the injector behavior. A wider annulus induces a larger spreading angle of the liquid-oxygen stream, which intercepts the kerosene stream in a more efficient way. Increasing the annulus width, however, imposes a wake region in a broader zone. The resultant flame becomes relatively unstable if the flame thickness is larger than the liquid-oxygen post thickness. Variation of the kerosene annulus width has a negligible effect on the dominant frequency of the pressure fluctuation, but it changes the amplitude of fluctuation.

Nomenclature

l_1	=	axial length of inner swirler
l_2	=	axial length of outer swirler
$\dot{m}_1$	=	mass flow rate of oxygen
$\dot{m}_2$	=	mass flow rate of kerosene
p'	=	pressure fluctuation
p_{cr}	=	critical pressure
p_0	=	chamber pressure
R	=	radius of discharge nozzle
R_{in}	=	radius of tangential inlet
R_v	=	radius of vortex chamber
r	=	radial coordinate
T	=	temperature
T_{cr}	=	critical temperature
T_{in}	=	temperature of tangential inlet
u_x	=	axial velocity component
u_θ	=	azimuthal velocity component
x	=	axial coordinate
Z	=	mixture fraction
Δr	=	annulus width
θ	=	phase angle
ρ	=	density
$\|\|\omega\|\|$	=	vorticity magnitude

I. Introduction

SWIRL injectors are widely used to achieve efficient mixing and combustion in propulsion and power-generation systems, including airbreathing engines [1,2] and liquid rockets [3]. The swirling motion of the injected fluid can improve flame stability by producing toroidal recirculation zones and reduce combustion length by inducing high rates of entrainment of the ambient fluid and fast mixing [4]. Injectors have strong effects on the stability characteristics of the combustion system because all feedback coupling of the combustion chamber with other engine components takes place through the injection process [5,6]. The situation becomes more complex when the engine operates at pressures higher than the critical pressures of the propellants [7]. The ensuing complexity of the underlying physics presents significant challenges to high-fidelity diagnostics and modeling/simulation.

Substantial experimental [8–12] and numerical [13–15] efforts on the characterization of propellant injection, mixing, and combustion processes at near- and supercritical conditions have recently led to improved understanding of the mechanisms involved. Most of these studies, however, have focused on shear coaxial injectors with light fluids, such as hydrogen and methane, as fuel. The situation in swirl injectors using kerosene, such as those widely used in Russian rocket engines like the RD-0110, RD-107/108, and RD 170/180, has not been explored in detail. For reference, the critical properties of oxygen and kerosene are listed in Table 1.

Existing experimental studies have focused on stability characteristics of oxygen and kerosene combustion system at various conditions. Miller et al. [16] investigated the combustion dynamics of the oxygen/kerosene system in a gas-centered, liquid-swirled coaxial injector with a chamber pressure range of 2.14–2.38 MPa. The stability behavior of the test rig as a function of chamber length was experimentally determined. The most amplified mode changes from the first longitudinal for the 38.1 cm chamber to the third longitudinal for the 88.9 cm chamber. Ahn et al. [17] examined the effect of the recess length of the center post and chamber pressure on the combustion dynamics of a liquid-oxygen (LOX)/kerosene bi-swirl injector. The inlet temperature of both LOX and kerosene streams remained subcritical, whereas the chamber pressure varied from 42 to 54 bar. It was found that the propellant mixing shifts from an external to an internal mode when the recess length exceeds a threshold value. In the internal mixing case, the amplitude of pressure fluctuations decreases as the chamber pressure transits from the subcritical to the supercritical state of oxygen. This behavior was not observed in the external mixing mode. At subcritical chamber pressures, the magnitude of pressure oscillations increases significantly with recess length, but at supercritical conditions, the recess length has negligible impact on pressure oscillation.

The limitations of optical diagnostics in the flame zone in experiments, however, restrict our understanding of the detailed flow and flame evolution, especially in the flame anchoring region. The present work attempts to provide detailed information about the flow and flame evolution of a LOX/kerosene biswirl injector under the supercritical conditions typical of contemporary rocket engines. A unified theoretical and numerical framework based on the large-eddy simulation technique is implemented. Fundamental physiochemical processes associated with propellant mixing and flame stabilization

Received 19 March 2016; revision received 26 May 2016; accepted for publication 26 May 2016; published online Open Access 28 July 2016.

*Graduate Research Assistant, School of Aerospace Engineering. Student Member AIAA

†William R. T. Oakes Professor and Chair, School of Aerospace Engineering; vigor.yang@aerospace.gatech.edu. Fellow AIAA (Corresponding author).

and spreading are explored, with special attention to the near-field development in the recess region downstream of the LOX post. The effect of kerosene annulus width on combustion performance is examined in depth, to provide support for future injector design.

II. Theoretical and Numerical Framework

The theoretical basis of the present study is described in Oefelein and Yang [18], which deals with supercritical fluid flows and combustion over the entire range of fluid thermodynamic states of concern. Turbulence closure is achieved using the large-eddy simulation technique. The Smagorinsky eddy viscosity model proposed by Erlebacher et al. [19] is employed to represent the effects of subgrid-scale motion. Thermodynamic properties, including density, enthalpy, and specific heat at constant pressure, are evaluated according to the modified Soave–Redlich–Kwong (SRK) equation of state (EOS) and fundamental thermodynamic theories. SRK EOS is used here for its validity over a broad range of fluid states and easy implementation. Transport properties, including thermal conductivity and dynamic viscosity, are estimated according to an extended corresponding-state principle. Mass diffusivity is obtained by the Takahashi method calibrated for high-pressure conditions [20]. The evaluation of thermodynamic and transport properties has been validated and implemented in previous studies [21–24].

Modeling of turbulence/chemistry interaction remains a critical issue, and an accurate and efficient treatment is yet to be established, even for ideal-gas mixtures. The situation is more challenging for real fluids because of thermodynamic nonidealities and transport anomalies in the transcritical regime. In light of these limitations, a simplified approach based on a steady laminar flamelet model is implemented in the present work. The assumption that the chemical length scale is smaller than the Kolmogorov scale is justified in the present high-pressure case, in which the flame zone is very thin [14].

The numerical framework was established by implementing a preconditioning scheme and a unified treatment of general-fluid thermodynamics [25]. It employs a density-based, finite volume methodology, along with a dual-time-step integration technique [26]. Temporal discretization is achieved using a second-order backward difference, and the inner-loop pseudotime term is integrated with a four-step Runge–Kutta scheme. Spatial discretization is obtained using a fourth-order central difference scheme in generalized coordinates. Fourth-order matrix dissipation, developed by Swanson and Turkel [27], is taken to ensure numerical stability and minimum contamination of the solution. Finally, a multiblock domain decomposition technique associated with the message-passing interface technique of parallel computing is applied to optimize computation speed.

III. Injector Configuration and Boundary Conditions

Figure 1 shows the liquid–liquid biswirl injector of concern, mimicking the RD-0110 engine, which powered the third stage of early versions of the Soyuz space vehicle. LOX is injected tangentially into the vortex chamber, whereas kerosene is delivered tangentially into the coaxial annulus of the injector. Figure 1b exhibits the major components: tangential inlets, a discharge nozzle, a vortex chamber, and a coaxial annulus. The baseline geometrical parameters and operating conditions are summarized in Table 2. The subscripts 1 and 2 represent LOX and kerosene, respectively. The thickness of the LOX post is 0.8 mm.

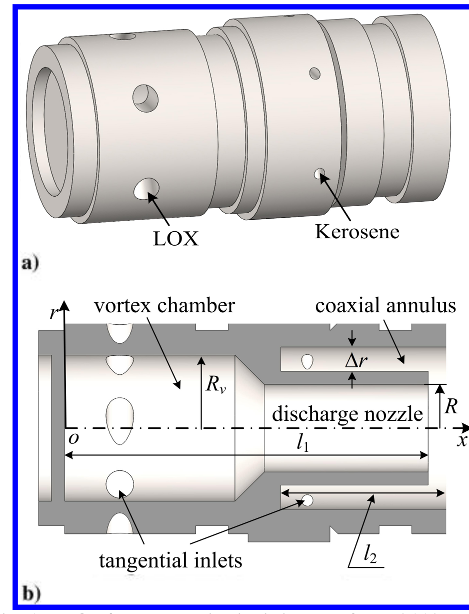

Fig. 1 LOX/kerosene biswirl injector of RD-0110 engine.

The computational domain includes the injector interior ($8.4R$ in the axial direction) and downstream region ($25R$ and $8R$ in the axial and radial directions, respectively). Because of the enormous computational effort required for calculating the flow evolution in the entire regime, only a cylindrical sector with periodic boundary conditions specified in the azimuthal direction is treated. This axisymmetric simplification introduces several limitations: 1) all tangential inlets (six each for oxidizer and fuel) are modeled using slits on the radial boundary of the injector; 2) flow variations in the azimuthal direction are neglected; and 3) the vortex-stretching mechanism, responsible for turbulent energy transfer from large to small eddies, is not included. In spite of these limitations, previous studies have shown that the present method of numerical analysis is able to capture primary characteristics of supercritical fluid injection and mixing, including density stratification, interfacial instability, and thermodynamic nonidealities [21,28]. The predicted values of film thickness and spreading angle show trends consistent with classical theory. Several important unsteady flow features, including interactions between hydrodynamic instabilities and acoustic oscillations, are explored in some depth. A full-scale three-dimensional simulation is computationally prohibitive for high Reynolds numbers, but the simulation presented here can quantitatively identify main features of swirling fluid mixing and combustion at supercritical pressure.

The no-slip and adiabatic boundary conditions are applied at the injector solid surface. At the inlets, the azimuthal and radial velocities are determined from the given mass flow rate and swirl strength. Pressure is obtained from the radial momentum equation. At the downstream boundary, nonreflecting boundary conditions based on the characteristic equations proposed by Poinsot and Lele [29] are applied to avoid undesirable wave reflection by extrapolation of primitive variables from the interior region. A reference pressure is applied to preserve the average pressure in the computational domain.

Table 1 Critical properties of oxygen and kerosene

Propellant	T_{cr}, K	p_{cr}, MPa
Oxygen	154.6	5.05
Kerosene	662.7	2.17

IV. Results and Discussion

A three-component surrogate model, n-decane/n-propylbenzene/n-propylcyclohexane (74%/15% /11% by volume), which has been shown to yield good agreement with the jet-stirred reactor data

Table 2 Geometric parameters and operating conditions

R_v	R	$R_{in,1}$	$R_{in,2}$	Δr	p_0	$T_{in,1}$	$T_{in,2}$	$\dot{m}_1$	$\dot{m}_2$	l_1	l_2
4.5 mm	2.7 mm	0.85 mm	0.35 mm	0.5 mm	10 MPa	120 K	300 K	0.15 kg/s	0.065 kg/s	22.7 mm	10.5 mm

Table 3 Grid parameters for four levels

Level	Minimum grid size, μm	Total meshes	Blocks
1	8	100,000	93
2	4	400,000	372
3	2	1,600,000	372
4	1	6,400,000	1488

[30,31], is employed to simulate the physicochemical behavior of kerosene. An associated reduced chemical mechanism including 106 species and 382 reactions is implemented because of its reasonable accuracy in predicting global combustion characteristics in terms of detailed profiles of species concentrations, ignition delay, and laminar flame speed [32]. A laminar flamelet library is established by tabulating the solutions of counterflow diffusion flames [24]. The injector flow and flame dynamics are studied in detail, with emphasis on the near-field mixing and flame stabilization mechanisms. The effect of the width of the kerosene annulus Δr is examined by treating two different designs at the same operating conditions; case 1 has annulus width 0.5 mm, and case 2 has annulus width 1.0 mm.

A. Grid-Independence Study

Previous studies [21,33] have shown that the results predicted by the present numerical scheme were consistent with experimental results [34] in cryogenic shear layers under both subcritical and supercritical conditions. Because of the unavailability of experimental data in literature, the numerical results based on current swirl-injector configuration could not be validated against experiments. To ensure appropriate numerical resolution of the underlying flow physics, a grid-independence study for case 1 was undertaken to determine the required grid spacing. Four different levels of mesh resolution were examined under cold-flow conditions; parameters are listed in Table 3. The grid size decreases by half as the grid level increases by one. The iterative time step must decrease accordingly to ensure numerical convergence. The total number of grid points increases from 0.1 million (level 1) to 6.4 million (level 4). The entire computational domain is divided into 93 (level 1) to 1488 (level 4) blocks, and each block is computed by one CPU core. For grid level 4, the resolution is close to direct numerical simulation, with the smallest grid size (1 μm) being on the order of magnitude of the Kolmogorov scale.

To examine the sensitivity of the calculated flow physics to grid resolution, the radial distributions of representative time-averaged flow properties, including the axial velocity u_x, temperature T, kerosene mass fraction y_F, and density ρ at $x/R = 10$, were compared for different grid resolutions, as shown in Fig. 2. The coarse grid level 1 shows significant differences from other levels. Although there are some slight distinctions between level 2 and levels 3 and 4, the averaged properties are nearly independent of grid resolution beyond level 2. Level 3 was thus selected as a tradeoff between computational accuracy and CPU hours. The smallest grid size is 2 μm, compared the Taylor scale of 8.4 μm in the LOX and kerosene shear layers downstream of the LOX post.

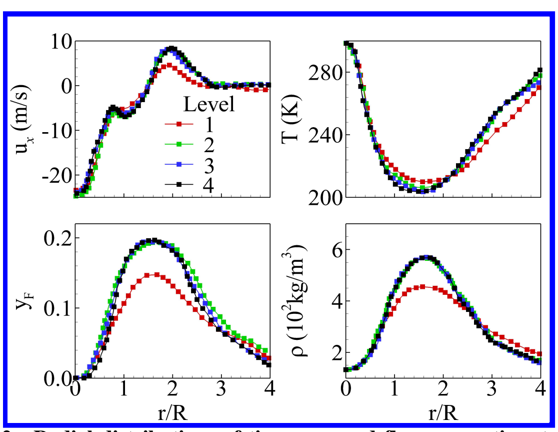

Fig. 2 Radial distributions of time-averaged flow properties at axial location $x/R = 10$ with increasing grid resolution.

B. Cold-Flow Dynamics

Calculations were first performed to study cold-flow mixing and dynamics. Figure 3 shows the instantaneous distributions of axial velocity u_x, density ρ, temperature T, and vorticity magnitude $|\omega|$ when the flowfield has reached its stationary state. (The flow dynamics associated with LOX swirlers without coflow kerosene were investigated in our previous studies [28,35,36].) Here, the strong swirling motion and its ensuing centrifugal force produce large pressure gradients in the radial direction and lead to the development of a LOX film flowing along the injector wall. A low-density gaseous core forms in the center region, due to the conservation of mass and angular momentum. The LOX film then exits the inner swirler, spreads outward, and impinges on the kerosene stream emanating from the outer swirler. Vigorous mixing of the LOX and kerosene occurs while the flow convects downstream. The axial velocity of the LOX film begins low near the injector headend in the vortex chamber and increases substantially through the converging nozzle; this can be attributed to the momentum transfer from the angular to the axial component. The LOX film thickness in the discharge nozzle decreases accordingly to satisfy mass conservation. The center recirculation induced by vortex breakdown downstream of the inner swirler renders a flow reversal in the gaseous core, leading to a strong shear layer between the LOX film and the core region.

The wider kerosene annulus in case 2 exerts substantial influence on the flow evolution in the recess region. The kerosene film does not cover the whole LOX post as it does in case 1; the thermal protection for the LOX post is not fully enforced, as will be shown later in the

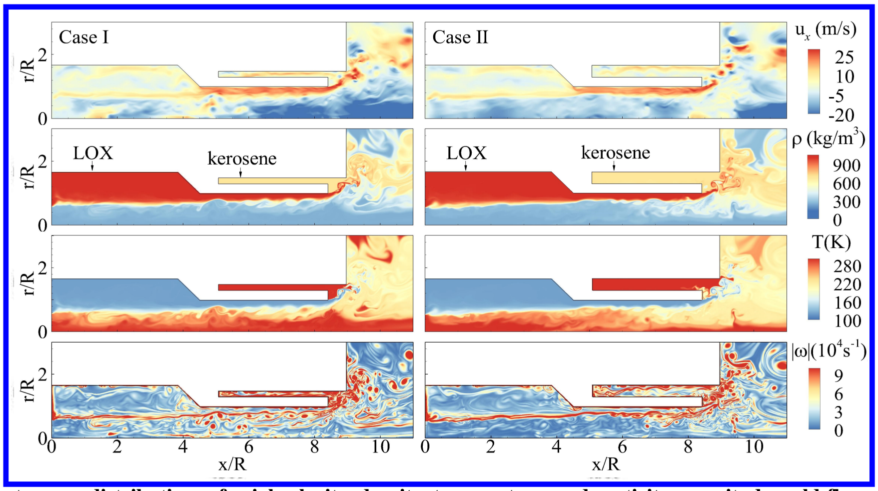

Fig. 3 Instantaneous distributions of axial velocity, density, temperature, and vorticity magnitude: cold-flow cases 1 and 2.

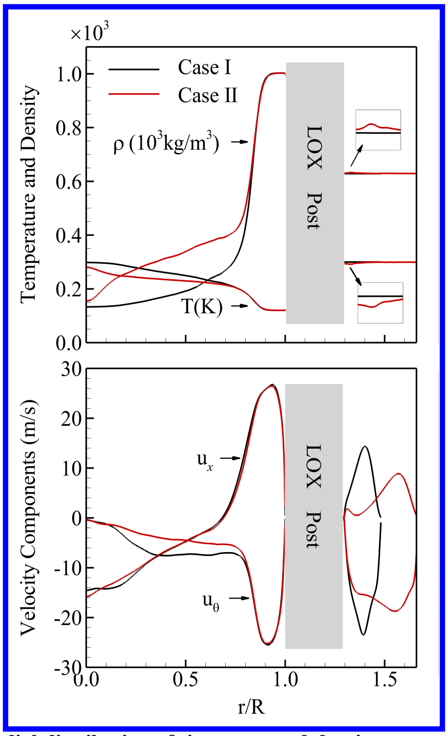

Fig. 4 Radial distribution of time-averaged density ρ, temperature T, and axial (u_x) and azimuthal velocity (u_θ) components slightly upstream of injector exit ($x/R = 8.3$): cold-flow cases 1 and 2.

reacting case. Case 2, however, produces a larger spreading angle in the LOX stream (54 deg versus 42 deg for case 1), intercepting the kerosene stream in a more efficient way. Strong vorticity takes place in the boundary layers near the walls and along the interface between the dense liquid and light gas in the inner swirler. The interfacial layer is intrinsically unstable. The associated longitudinal waves develop to large-scale billows, which, in turn, enhance the thermal mixing of the LOX film and gaseous oxygen. The vortical field becomes extremely dynamic in the recess region because of propellant mixing and shear-layer instability.

Figure 4 presents the time-averaged density, temperature, and velocity components slightly upstream of the injector exit. The temperature changes gradually from subcritical at the wall ($T = 120$ K, $r/R = 1$) to supercritical in the center ($T = 300$ K, $r/R = 0$). A fluid transition region exists, unlike the sharp interface found between a liquid and a gas at subcritical pressures. Followed by this change of fluid state, the density varies smoothly from a large value in the LOX film to a small value in the gaseous core. In the inner swirler, the distributions of flow properties for cases 1 and 2 are quite similar around the LOX film. Slight differences are found in the distributions in the gaseous core, due to the effect of center-recirculating flow downstream of the injector post. The radial distributions of density and temperature in the kerosene annulus ($r/R \geq 1.3$) are uniform for case 1. Slight nonuniformity in case 2 appears near the bottom surface of the annulus ($r/R \sim 1.3$) due to the penetration of LOX. The velocity profiles, however, show significant differences between the two cases. The narrower annulus in case 1 produces a symmetric profile for both axial and azimuthal components, with the maximum in the center of the annulus. The peak values of respective components in case 2 are smaller and close to the outer wall of the annulus.

C. Reacting-Flow Dynamics

Figure 5 shows the instantaneous distributions of temperature T, mixture fraction Z (defined as the mass fraction of C and H atoms), and mass fraction of H_2O (y_{H_2O}) in the vicinity of the inner swirler exit. A diffusion-dominated flame emanates from the recess region and propagates downstream along the surface of the LOX stream. A wake region consisting of hot combustion products separates the LOX from the kerosene stream. Large-scale vortices induced by shear-layer instability wrinkle the flame in the downstream region, where center-recirculation is generated by vortex breakdown and induces the flow reversal of hot products near the centerline of the injector.

In case 1, unlike the cold-flow case shown in Fig. 3, in which the recess region is occupied by the kerosene stream, the hot products produced by combustion expand in all directions and force the kerosene to flow along the upper surface of the injector and the LOX post. The mixture in these areas is very kerosene-rich. As a result, the flame zone is not attached to the LOX post surface and the slight lifting of the flame may offer some thermal protection to the LOX post. In case 2, however, the flame is attached to the LOX post, where the mixture fraction is close to stoichiometric ($Z_{st} = 0.225$), impos-

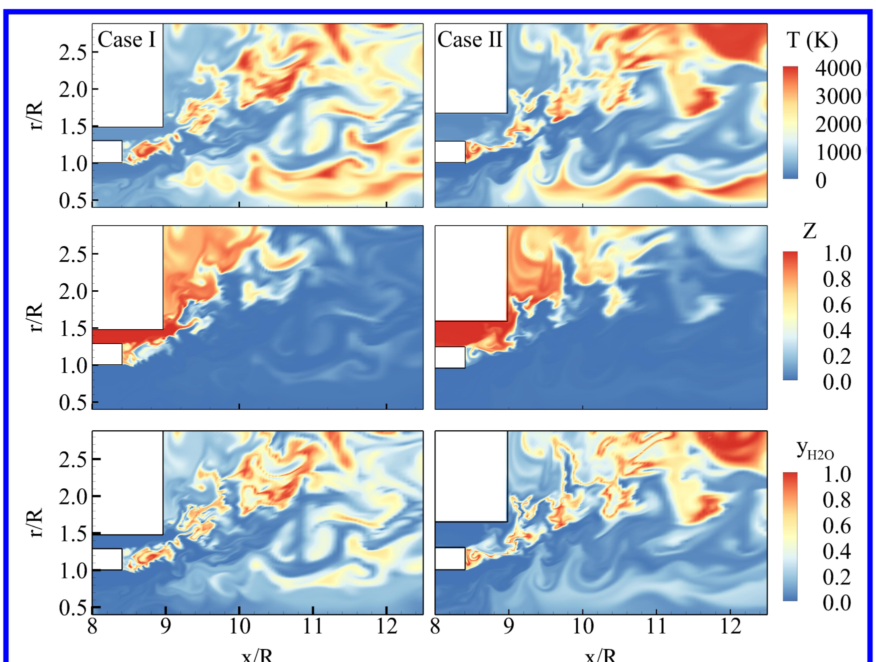

Fig. 5 Instantaneous distributions of temperature, mixture fraction, and water mass fraction immediately downstream of the inner injector exit: combustion cases 1 and 2.

ing a significant heat flux on the LOX post. Downstream of the injector, the hot products further drive the kerosene stream flowing along the injector faceplate, unlike the cold-flow case that develops a well-distributed mixture propagating downstream. The kerosene film may protect the faceplate from overheat caused by recirculating hot products.

Flame stabilization is a critical issue in combustor design. Zong and Yang [14] and Oefelein and Yang [18] have shown that the flame is stabilized by the recirculating flow downstream of the LOX post in a shear coaxial injector with cryogenic propellants. A similar phenomenon is observed for the liquid biswirl injector in the present study. The flame is initiated and anchored in the wake region behind the LOX post, where two counter-rotating recirculation zones form, as shown in Fig. 6. The upper bubble is a kerosene-rich mixture, and the lower one is an oxygen-rich mixture, due to the diffusion process. This low-velocity region provides the primary flame-holding mechanism. Another two recirculating regions are generated near the injector faceplate and along the centerline (not shown). They play an important role in stabilizing combustion by preheating the incoming kerosene and LOX. All these recirculating flows act as a hot-product pool providing energy to ignite fresh propellants and sustain the flame.

The wider kerosene annulus in case 2 produces larger recirculating bubbles (1.19 mm in the radial direction versus 0.84 mm in case 1) in the recess region and therefore distributes the flame in a broader zone. The upper bubble penetrates into the annulus, blocks the flow passage, and leads to flow reversal near the lower surface of the annulus. This unique flow structure may transport oxygen into the annulus and generate a flame attached to the inner surface of the annulus.

The oscillatory flowfield was carefully investigated to gain insight into the mechanisms driving acoustic oscillations. Virtual probes were placed at a number of locations to record the flow motions. Figure 7 shows the pressure fluctuations p' in both time and frequency space downstream of the LOX post, at the location denoted in the figure by a black dot. The pressure oscillates periodically due to the strong interactions of the vortices and their coupling with the flame. The maximum amplitude of the relative pressure, defined as p'/p_0, is less than 10% for both cases, but the amplitude in case 2 is considerably higher. The power spectral density reveals the same dominant frequency (6.47 kHz) for both cases, corresponding to the vortex shedding frequency. This can be explained by the similar velocity profiles of cases 1 and 2 emanating from the inner swirler, which induce similar inner shear layers between the LOX stream and the hot products. The variation of the kerosene annulus width has a negligible effect on the dominant vortex-shedding frequency, but it

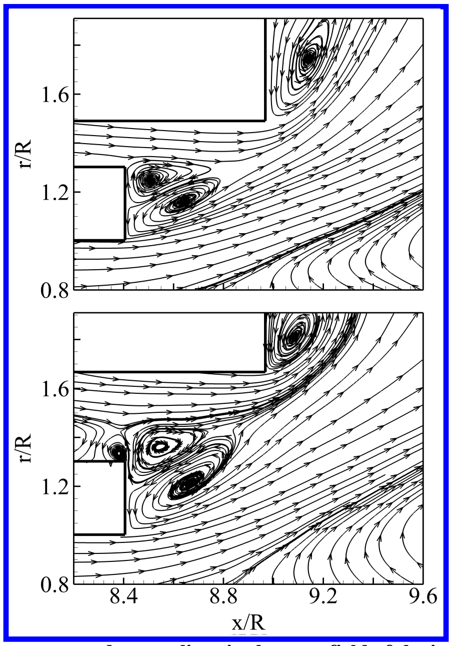

Fig. 6 Time-averaged streamlines in the near field of the inner swirler exit: combustion cases 1 and 2.

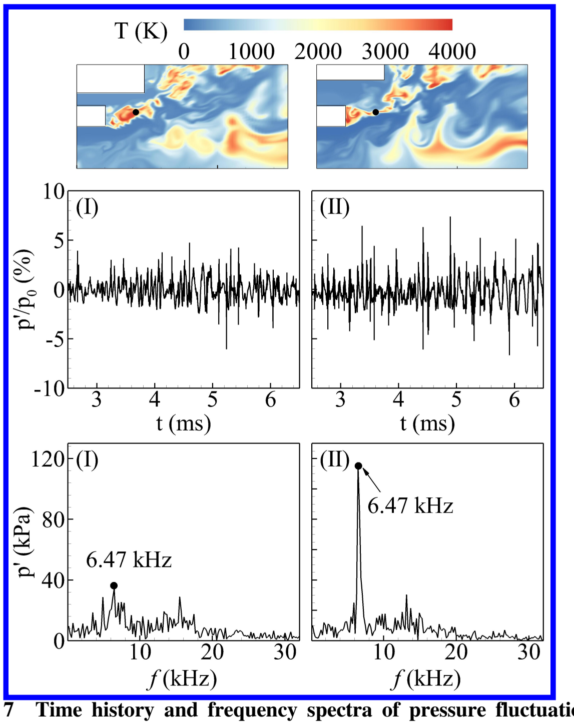

Fig. 7 Time history and frequency spectra of pressure fluctuation: combustion cases 1 and 2.

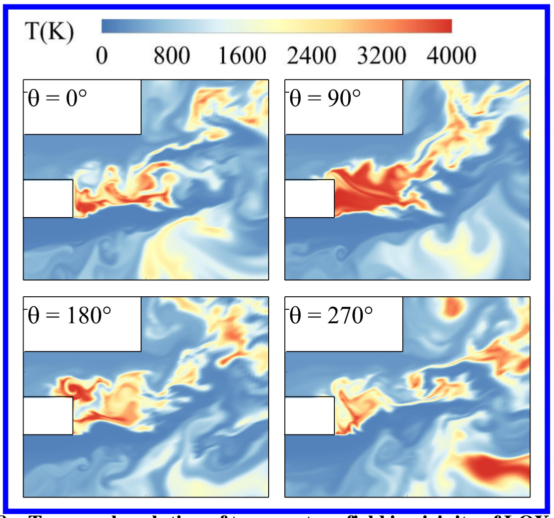

Fig. 8 Temporal evolution of temperature field in vicinity of LOX post: combustion case 2.

determines the amplitude of fluctuation. Further analysis of heat-release-rate oscillations induced by acoustic and vortical perturbations will be presented in subsequent work on underlying flame responses.

Figure 8 shows the temporal evolution of the temperature field near the LOX post for case 2 over one cycle of vortex shedding, where θ is referenced to the phase angle with respect to the pressure oscillation at the end of the LOX post. The flame evolves under the influence of the vortical flow. The flame is initiated at the LOX post and intensified in the recess region, is then pushed upstream into the annulus by recirculating flows, and is eventually extinguished by the incoming cold kerosene stream. This process may be contributed to the flame overexposure to the kerosene stream because the flame thickness is larger than the post thickness [37]. This unstable flame behavior may generate and modify flow oscillations in the injector.

V. Conclusions

The mixing and combustion dynamics of liquid-oxygen (LOX)/kerosene biswirl injectors at supercritical pressure were investigated by implementing a unified theoretical and numerical framework for general fluids. Turbulent closure was achieved using the large-eddy simulation technique along with a laminar flamelet library approach. The numerical accuracy of the current simulations was tested through a grid-independence study. In the configuration under consideration, the flame is stabilized by multiple recirculating zones: two counter-rotating vortices in the recess region, center-recirculation downstream of the injector, and corner-recirculation at the injector faceplate. These zones act as a hot-product pool, providing energy to ignite incoming propellants and sustain the flame. The width of the kerosene annulus has a significant effect on the flow evolution and flame propagation in the vicinity of the LOX post. With the narrower annulus, the flame is lifted slightly off the post, which is covered by the kerosene film to provide thermal protection. In the case with a wider annulus, the flame is closely attached to the post, and the intensive heat flux at the post wall significantly increases the temperature of the post surface. The annulus width is found to exert little influence on the dominant frequency of flow oscillation, but it plays an important role in determining the amplitude of wave motion. Furthermore, the wider annulus generates a larger recirculating region in the vicinity of the LOX post and introduces flame on the inner surface of the annulus. This flame is readily extinguished, due to its overexposure to the kerosene stream.

Acknowledgments

This work was sponsored by the U.S. Air Force Office of Scientific Research under grant FA 9550-10-1-0179. The authors gratefully acknowledge support and advice from Mitat A. Birkan.

References

[1] Lieuwen, T. C., and Yang, V., (eds.), *Combustion Instabilities in Gas Turbine Engines (Operational Experience, Fundamental Mechanisms and Modeling)*, Vol. 210, Progress in Astronautics and Aeronautics, AIAA, Reston, VA, 2005. doi:10.2514/4.866807

[2] Huang, Y., and Yang, V., "Dynamics and Stability of Lean-Premixed Swirl-Stabilized Combustion," *Progress in Energy and Combustion Science*, Vol. 35, No. 4, 2009, pp. 293–364. doi:10.1016/j.pecs.2009.01.002

[3] Bazarov, V., Yang, V., and Puri, P., "Design and Dynamics of Jet and Swirl Injectors," *Liquid Rocket Thrust Chambers: Aspects of Modeling, Analysis, and Design*, edited by Yang, V., Habiballah, M., Hulka, J., and Popp, M., Vol. 200, Progress in Astronautics, and Aeronautics, AIAA, Reston, VA, 2004, pp. 19–103. doi:10.2514/4.866760

[4] Syred, N., "A Review of Oscillation Mechanisms and the Role of the Precessing Vortex Core (PVC) in Swirl Combustion Systems," *Progress in Energy and Combustion Science*, Vol. 32, No. 2, 2006, pp. 93–161. doi:10.1016/j.pecs.2005.10.002

[5] Bazarov, V. G., and Yang, V., "Liquid-Propellant Rocket Engine Injector Dynamics," *Journal of Propulsion and Power*, Vol. 14, No. 5, 1998, pp. 797–806. doi:10.2514/2.5343

[6] Ahn, K., and Choi, H.-S., "Combustion Dynamics of Swirl Coaxial Injectors in Fuel-Rich Combustion," *Journal of Propulsion and Power*, Vol. 28, No. 6, 2012, pp. 1359–1367. doi:10.2514/1.B34448

[7] Yang, V., "Modeling of Supercritical Vaporization, Mixing, and Combustion Processes in Liquid-Fueled Propulsion Systems," *Proceedings of the Combustion Institute*, Vol. 28, No. 1, 2000, pp. 925–942. doi:10.1016/S0082-0784(00)80299-4

[8] Mayer, W., and Tamura, H., "Propellant Injection in a Liquid Oxygen/Gaseous Hydrogen Rocket Engine," *Journal of Propulsion and Power*, Vol. 12, No. 6, 1996, pp. 1137–1147. doi:10.2514/3.24154

[9] Candel, S., Juniper, M., Singla, G., Scouflaire, P., and Rolon, C., "Structure and Dynamics of Cryogenic Flames at Supercritical Pressure," *Combustion Science and Technology*, Vol. 178, Nos. 1–3, 2006, pp. 161–192. doi:10.1080/00102200500292530

[10] Lux, J., and Haidn, O., "Flame Stabilization in High-Pressure Liquid Oxygen/Methane Rocket Engine Combustion," *Journal of Propulsion and Power*, Vol. 25, No. 1, 2009, pp. 15–23. doi:10.2514/1.36852

[11] Roy, A., and Segal, C., "Experimental Study of Fluid Jet Mixing at Supercritical Conditions," *Journal of Propulsion and Power*, Vol. 26, No. 6, 2010, pp. 1205–1211. doi:10.2514/1.48462

[12] Schmitt, T., Rodriguez, J., Leyva, I., and Candel, S., "Experiments and Numerical Simulation of Mixing Under Supercritical Conditions," *Physics of Fluids*, Vol. 24, No. 5, 2012, Paper 055104. doi:10.1063/1.3701374

[13] Oefelein, J. C., "Thermophysical Characteristics of Shear-Coaxial LOX–H2 Flames at Supercritical Pressure," *Proceedings of the Combustion Institute*, Vol. 30, No. 2, 2005, pp. 2929–2937. doi:10.1016/j.proci.2004.08.212

[14] Zong, N., and Yang, V., "Near-Field Flow and Flame Dynamics of LOX/Methane Shear-Coaxial Injector Under Supercritical Conditions," *Proceedings of the Combustion Institute*, Vol. 31, No. 2, 2007, pp. 2309–2317. doi:10.1016/j.proci.2006.08.106

[15] Bellan, J., "Theory, Modeling and Analysis of Turbulent Supercritical Mixing," *Combustion Science and Technology*, Vol. 178, Nos. 1–3, 2006, pp. 253–281. doi:10.1080/00102200500292241

[16] Miller, K., Sisco, J., Nugent, N., and Anderson, W., "Combustion Instability with a Single-Element Swirl Injector," *Journal of Propulsion and Power*, Vol. 23, No. 5, 2007, pp. 1102–1112. doi:10.2514/1.26826

[17] Ahn, K., Han, Y.-M., Seo, S., and Choi, H.-S., "Effects of Injector Recess and Chamber Pressure on Combustion Characteristics of Liquid–Liquid Swirl Coaxial Injectors," *Combustion Science and Technology*, Vol. 183, No. 3, 2010, pp. 252–270. doi:10.1080/00102202.2010.516289

[18] Oefelein, J. C., and Yang, V., "Modeling High-Pressure Mixing and Combustion Processes in Liquid Rocket Engines," *Journal of Propulsion and Power*, Vol. 14, No. 5, 1998, pp. 843–857. doi:10.2514/2.5349

[19] Erlebacher, G., Hussaini, M., Speziale, C., and Zang, T. A., "Toward the Large-Eddy Simulation of Compressible Turbulent Flows," *Journal of Fluid Mechanics*, Vol. 238, May 1992, pp. 155–185. doi:10.1017/S0022112092001678

[20] Takahashi, S., "Preparation of a Generalized Chart for the Diffusion Coefficients of Gases at High Pressures," *Journal of Chemical Engineering of Japan*, Vol. 7, No. 6, 1975, pp. 417–420. doi:10.1252/jcej.7.417

[21] Zong, N., Meng, H., Hsieh, S. Y., and Yang, V., "A Numerical Study of Cryogenic Fluid Injection and Mixing Under Supercritical Conditions," *Physics of Fluids*, Vol. 16, No. 12, 2004, pp. 4248–4261. doi:10.1063/1.1795011

[22] Wang, X., Huo, H., and Yang, V., "Supercritical Combustion of General Fluids in Laminar Counterflows," *51st AIAA Aerospace Sciences Meeting*, AIAA Paper 2013-1165, Jan. 2013. doi:10.2514/6.2013-1165

[23] Huo, H., Wang, X., and Yang, V., "A General Study of Counterflow Diffusion Flames at Subcritical and Supercritical Conditions: Oxygen/Hydrogen Mixtures," *Combustion and Flame*, Vol. 161, No. 12, 2014, pp. 3040–3050. doi:10.1016/j.combustflame.2014.06.005

[24] Wang, X., Huo, H., and Yang, V., "Counterflow Diffusion Flames of Oxygen and N-Alkane Hydrocarbons (CH4-C16H34) at Subcritical and Supercritical Conditions," *Combustion Science and Technology*, Vol. 187, Nos. 1–2, 2015, pp. 60–82. doi:10.1080/00102202.2014.973955

[25] Meng, H., and Yang, V., "A Unified Treatment of General Fluid Thermodynamics and Its Application to a Preconditioning Scheme," *Journal of Computational Physics*, Vol. 189, No. 1, 2003, pp. 277–304. doi:10.1016/S0021-9991(03)00211-0

[26] Hsieh, S.-Y., and Yang, V., "A Preconditioned Flux-Differencing Scheme for Chemically Reacting Flows at all Mach Numbers," *International Journal of Computational Fluid Dynamics*, Vol. 8, No. 1, 1997, pp. 31–49. doi:10.1080/10618569708940794

[27] Swanson, R. C., and Turkel, E., "On Central-Difference and Upwind Schemes," *Journal of Computational Physics*, Vol. 101, No. 2, 1992, pp. 292–306. doi:10.1016/0021-9991(92)90007-L

[28] Zong, N., and Yang, V., "Cryogenic Fluid Dynamics of Pressure Swirl Injectors at Supercritical Conditions," *Physics of Fluids*, Vol. 20, No. 5, 2008, Paper 056103, doi:10.1063/1.2905287

[29] Poinsot, T. J., and Lele, S. K., "Boundary Conditions for Direct Simulations of Compressible Viscous Flows," *Journal of Computa-*

tional Physics, Vol. 101, No. 1, 1992, pp. 104–129.
doi:10.1016/0021-9991(92)90046-2

[30] Dagaut, P., "On the Kinetics of Hydrocarbons Oxidation from Natural Gas to Kerosene and Diesel Fuel," Physical Chemistry Chemical Physics, Vol. 4, No. 11, 2002, pp.2079-2094
doi:10.1039/B110787A

[31] Dagaut, P., and Cathonnet, M., "The Ignition, Oxidation, and Combustion of Kerosene: A Review of Experimental and Kinetic Modeling," *Progress in Energy and Combustion Science*, Vol. 32, No. 1, 2006, pp. 48–92.
doi:10.1016/j.pecs.2005.10.003

[32] Wang, Q.-D., Fang, Y.-M., Wang, F., and Li, X.-Y., "Skeletal Mechanism Generation for High-Temperature Oxidation of Kerosene Surrogates," *Combustion and Flame*, Vol. 159, No. 1, 2012, pp. 91–102.
doi:10.1016/j.combustflame.2011.05.019

[33] Zong, N., and Yang, V., "Cryogenic Fluid Jets and Mixing Layers in Transcritical and Supercritical Environments," *Combustion Science and Technology*, Vol. 178, Nos. 1–3, 2006, pp. 193–227.
doi:10.1080/00102200500287613

[34] Chehroudi, B., Cohn, R., and Talley, D., "Cryogenic Shear Layers: Experiments and Phenomenological Modeling of the Initial Growth Rate Under Subcritical and Supercritical Conditions," *International Journal of Heat and Fluid Flow*, Vol. 23, No. 5, 2002, pp. 554–563.
doi:10.1016/S0142-727X(02)00151-0

[35] Wang, X., Huo, H., Wang, Y., Zhang, L., and Yang, V., "A Three-Dimensional Analysis of Swirl Injector Flow Dynamics at Supercritical Conditions," *53rd AIAA Aerospace Sciences Meeting*, AIAA Paper 2015-1827, 2015.
doi:10.2514/6.2015-1827

[36] Wang, X., and Yang, V., "Supercritical Injection and Mixing Characteristics of Liquid Oxygen/Kerosene Bi-Swirl Injectors," *54th AIAA Aerospace Sciences Meeting*, AIAA Paper 2016-1933, 2016.
doi:10.2514/6.2016-1933

[37] Juniper, M., and Candel, S., "Edge Diffusion Flame Stabilization Behind a Step over a Liquid Reactant," *Journal of Propulsion and Power*, Vol. 19, No. 3, 2003, pp. 332–341.
doi:10.2514/2.6134

J. C. Oefelein
Associate Editor

This article has been cited by:

1. Jeongseok Kang, Hong-Gye Sung. 2017. Kerosene/GOx dynamic combustion characteristics in a mixing layer under supercritical conditions using the LES-FPV approach. *Fuel* **203**, 579-590. [CrossRef]
2. Yixing Li, liyixing@gatech.edu Georgia Institute of Technology; Xingjian Wang, xwang343@gatech.edu Georgia Institute of Technology; Liwei Zhang, liwei@gatech.edu Georgia Institute of Technology; Shiang-Ting Yeh, syeh32@gatech.edu Georgia Institute of Technology; Vigor Yang, vigor.yang@aerospace.gatech.edu Georgia Institute of Technology Flow Dynamics of Gaseous Oxygen/Kerosene Jet-Swirl Injectors at Supercritical Conditions . [Citation] [PDF] [PDF Plus]
3. Suo Yang, syang305@gatech.edu Georgia Institute of Technology; Xingjian Wang, xwang343@gatech.edu Georgia Institute of Technology; Vigor Yang, vigor.yang@aerospace.gatech.edu Georgia Institute of Technology; Wenting Sun, wenting.sun@ae.gatech.edu Georgia Institute of Technology; Hongfa Huo, hongfa.huo@gmail.com Georgia Institute of Technology Comparison of Flamelet/Progress-Variable and Finite-Rate Chemistry LES Models in a Preconditioning Scheme . [Citation] [PDF] [PDF Plus]